The Astrophysical Journal, 677:1046–1059, 2008 April 20

THE SLOAN LENS ACS SURVEY. VI. DISCOVERY AND ANALYSIS OF A DOUBLE EINSTEIN RING[1]

Raphaël Gavazzi,[2] Tommaso Treu,[2,3,4] Léon V. E. Koopmans,[5] Adam S. Bolton,[6,7]
Leonidas A. Moustakas,[8] Scott Burles,[9] and Philip J. Marshall[2]
Received 2007 October 24; accepted 2008 January 14

ABSTRACT

We report the discovery of two concentric Einstein rings around the gravitational lens SDSS J0946+1006. The main lens is at redshift $z_l = 0.222$, while the inner ring (1) is at redshift $z_{s1} = 0.609$ ($R_{\rm Ein1} = 1.43'' \pm 0.01''$). The wider image separation ($R_{\rm Ein2} = 2.07'' \pm 0.02''$) of the outer ring (2) implies a higher redshift than that of ring 1; the detection of ring 2 in the F814W ACS filter implies an upper limit of $z_{s2} \lesssim 6.9$. The main lens can be described by a power-law total mass density profile $\rho_{\rm tot} \propto r^{-\gamma'}$ with $\gamma' = 2.00 \pm 0.03$ and velocity dispersion $\sigma_{\rm SIE} = 287 \pm 5$ km s^{-1} (the stellar velocity dispersion is $\sigma_{v,*} = 284 \pm 24$ km s^{-1}). The strong lensing configuration is inconsistent with light traces mass. Adopting a prior on the stellar mass-to-light ratio from previous SLACS work, we infer a 73% ± 9% dark matter fraction within the cylinder of radius equal to the effective radius of the lens. We find that, for the case of SDSS J0946+1006, the geometry of the two rings does not place interesting constraints on cosmography because of the suboptimal redshifts of lens and sources. We then consider the perturbing effect of the mass associated with ring 1 building a compound lens model. This introduces minor changes to the mass of the main lens and provides an estimate of $z_{s2} = 3.1^{+2.0}_{-1.0}$ and of the mass of the source responsible for ring 1 ($\sigma_{{\rm SIE},s1} = 94^{+27}_{-47}$ km s^{-1}). We conclude by examining the prospects of doing cosmography with a sample of 50 double rings, expected from future space-based surveys. Accounting for uncertainties in the mass profile of the lens and the effects of the perturber, we find that such a sample would constrain Ω_m and w within 10%, assuming flatness.

Subject headings: cosmological parameters — dark matter — galaxies: elliptical and lenticular, cD — galaxies: halos — galaxies: structure — gravitational lensing

Online material: color figures

1. INTRODUCTION

Measuring the mass distribution of galaxies is essential for understanding a variety of astrophysical processes. Extended mass profiles of galaxies provide evidence for dark matter using either rotation curves (e.g., Rubin et al. 1980; van Albada et al. 1985; Swaters et al. 2003), weak lensing (e.g., Brainerd et al. 1996; Hoekstra et al. 2004; Sheldon et al. 2004; Mandelbaum et al. 2006), or dynamics of satellite galaxies (e.g., Prada et al. 2003; Conroy et al. 2007), which is one of the main ingredients of the standard ΛCDM cosmological model. At galactic and subgalactic scales, numerical cosmological simulations make quantitative predictions regarding, e.g., the inner slope of mass density profiles and the existence of dark matter substructure. Precise mass measurements are key to test the predictions and provide empirical input to further improve the models.

Gravitational lensing has emerged in the last two decades as one of the most powerful ways to measure the mass distributions of galaxies, by itself or in combination with other diagnostics. Although strong gravitational lenses are relatively rare in the sky ($\lesssim$20 deg^{-2} at space-based depth and resolution; Marshall et al. 2005; Moustakas et al. 2007), the number of known galaxy-scale gravitational lens systems has increased well beyond 100 as a result of a number of dedicated efforts exploiting a variety of techniques (e.g., Warren et al. 1996; Ratnatunga et al. 1999; Kochanek et al. 1999; Myers et al. 2003; Bolton et al. 2004; Cabanac et al. 2007). The increased number of systems, together with the improvement of modeling techniques (e.g., Kochanek & Narayan 1992; Warren & Dye 2003; Treu & Koopmans 2004; Brewer & Lewis 2006; Suyu et al. 2006; Wayth & Webster 2006; Barnabè & Koopmans 2007), has enabled considerable progress not only in the use of this diagnostic for the study of the mass distribution of early and most recently late-type galaxies, but also for cosmography, i.e., the determination of cosmological parameters (e.g., Golse et al. 2002; Soucail et al. 2004; Dalal et al. 2005).

Given the already small optical depth for strong lensing, the lensing of multiple background sources by a single foreground galaxy is an extremely rare event. At *Hubble Space Telescope* (*HST*) resolution (FWHM $\sim 0.12''$) and depth ($I_{\rm AB} \sim 27$) it is expected that 1 massive early-type galaxy (which dominate the lensing cross section) in about 200 is a strong lens (Marshall et al. 2005). Taking into account the strong dependence of the lensing cross section on lens galaxy velocity dispersion ($\propto\sigma^4$) and the population of lens galaxies, we estimate that about one lens galaxy in ∼40−80 could be a double source plane strong gravitational lens (see the Appendix). For these reasons, at most a handful of double lenses are to be found in the largest spectroscopic surveys of early-type galaxies such as the luminous red galaxies of the Sloan Digital Sky Survey. However, future high-resolution imaging

[1] Based on observations made with the NASA/ESA *Hubble Space Telescope*, obtained at the Space Telescope Science Institute, which is operated by the Association of Universities for Research in Astronomy, Inc., under NASA contract NAS 5-26555. These observations are associated with program 10886. Support for program 10886 was provided by NASA through a grant from the Space Telescope Science Institute, which is operated by the Association of Universities for Research in Astronomy, Inc., under NASA contract NAS 5-26555.

[2] Department of Physics, University of California, Santa Barbara, CA 93106-9530.
[3] Sloan Fellow.
[4] Packard Fellow.
[5] Kapteyn Astronomical Institute, University of Groningen, 9700 AV Groningen, Netherlands.
[6] Institute for Astronomy, University of Hawaii, Honolulu, HI 96822.
[7] Harvard-Smithsonian Center for Astrophysics, Cambridge, MA 02138.
[8] Jet Propulsion Laboratory, California Institute of Technology, Pasadena, CA 91109.
[9] Department of Physics and Kavli Institute for Astrophysics and Space Research, Massachusetts Institute of Technology, Cambridge, MA 02139.

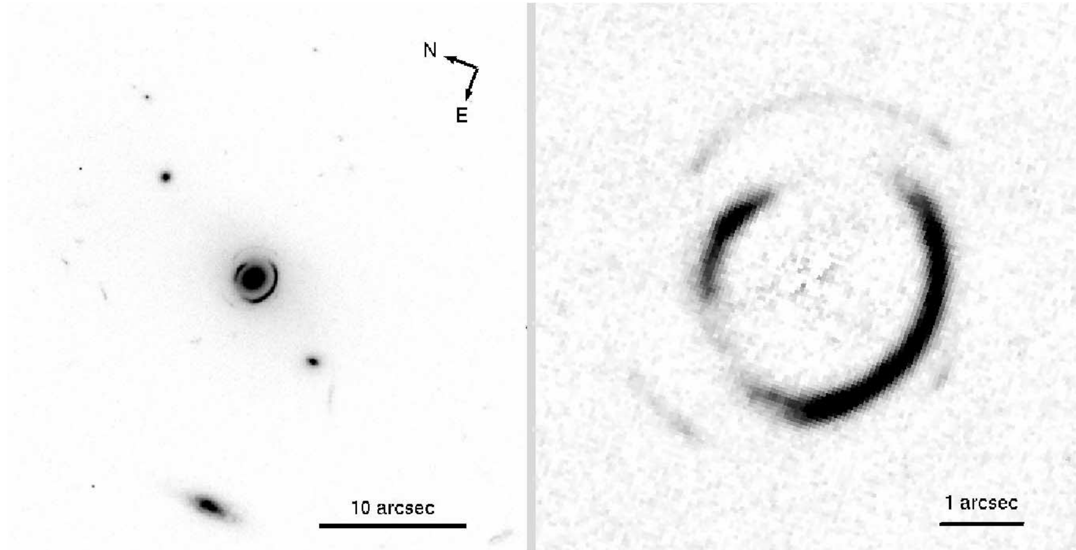

FIG. 1.—*HST* F814W overview of the lens system SDSS J0946+1006. The right panel is a zoom onto the lens showing two concentric partial ring–like structures after subtracting the lens surface brightness. [*See the electronic edition of the Journal for a color version of this figure.*]

surveys such as those planned for JDEM and DUNE (Aldering et al. 2004; Réfrégier et al. 2006) will increase the number of known lenses by 2–3 orders of magnitude (Marshall et al. 2005) and hence should be able to provide large statistical samples of double source plane gravitational lenses, opening up the possibility of qualitatively new applications of gravitational lensing for the study of galaxy formation and cosmography.

We report here the discovery of the first double source plane partial Einstein ring. The gravitational lens system SDSS J0946+1006 was discovered as part of the Sloan Lens ACS (SLACS) Survey (Bolton et al. 2005, 2006a, 2007; Treu et al. 2006; Koopmans et al. 2006; Gavazzi et al. 2007). The object was first selected by the presence of multiple emission lines at higher redshift in the residuals of an absorption-line spectrum from the SDSS database as described by Bolton et al. (2004) and then confirmed as a strong lens by high-resolution imaging with the Advanced Camera for Surveys (ACS) aboard *HST*. In addition to an Einstein ring due to the source (hereafter source 1) responsible for the emission lines detected in the SDSS spectrum, the Hubble image also shows a second multiply imaged system forming a broken Einstein ring with a larger diameter than the inner ring (hereafter source 2). This configuration can only arise if the two lensed systems are at different redshifts and well aligned with the center of the lensing galaxy. It is a great opportunity that a double source plane lens has been found among the approximately 90 lenses discovered by the SLACS collaboration to date (Bolton et al. 2008).

The goal of this paper is to study and model this peculiar system in detail, as an illustration of some astrophysical applications of double source plane compound lenses, including (1) the determination of the mass density profile of the lens galaxy independent of dynamical constraints, (2) placing limits on the mass of source 1 based on multiple lens plane modeling, and (3) estimating the redshift of source 2 and the cosmological parameters from the angular distance size ratios. The paper is therefore organized as follows. Section 2 summarizes the observations and photometric and spectroscopic measurements and discusses the morphology of the lens system. Section 3 describes our gravitational lens modeling methodology. Section 4 gives the main results in terms of constraints on the mass distribution of the lens galaxy and of source 1. Section 5 discusses the use of double source plane lenses as a tool for cosmography using the example of SDSS J0946+1006 and also addresses the potential of large samples of such double source plane lenses for the same purpose. In § 6 we summarize our results and briefly conclude.

Unless otherwise stated, we assume a concordance cosmology with $H_0 = 70\, h_{70}$ km s^{-1} Mpc^{-1}, $\Omega_m = 0.3$, and $\Omega_\Lambda = 0.7$. All magnitudes are expressed in the AB system.

2. DATA

The lens galaxy SDSS J0946+1006 was first identified in the spectroscopic SDSS database based on the redshift of the lensing galaxy $z_l = 0.222$ and that of a background source at $z_{s1} = 0.609$ (hereafter source 1), as described by Bolton et al. (2004, 2006a, 2008). This section describes *HST* follow-up imaging (§ 2.1), the properties of the lens (§ 2.2), and lensed galaxies (§ 2.3).

2.1. *Hubble Space Telescope Observations and Data Reduction*

SDSS J0946+1006 was then imaged with the ACS on board the *HST* (Cycle 15, Program 10886, PI Bolton). The Wide Field Channel with filter F814W was used for a total exposure time of 2096 s. Four subexposures were obtained with a semi-integer pixel offset (`acs-wfc-dither-box`) to ensure proper cosmic-ray removal and sampling of the point-spread function (PSF). The image reduction process is described in Gavazzi et al. (2007) and results in a $0.03''$ pixel^{-1} spatial sampling. This pixel size provides good sampling of the PSF for weak-lensing applications, at the (small) price of inducing noise correlation over scales of 1–2 pixels. This is accounted for in our analysis by correcting pixel variances according to the procedure described by Casertano et al. (2000).

Figure 1 shows the *HST* image of the lens galaxy field together with an enlarged view of the lensed features, after subtraction of a smooth model for the lens surface brightness distribution. For reference, $1''$ in the lens plane subtends a physical scale of $3.580\, h_{70}^{-1}$ kpc.

2.2. *Lens Galaxy Properties*

The two-dimensional lens surface brightness was fitted with GALFIT (Peng et al. 2002) using two elliptical Sérsic components.

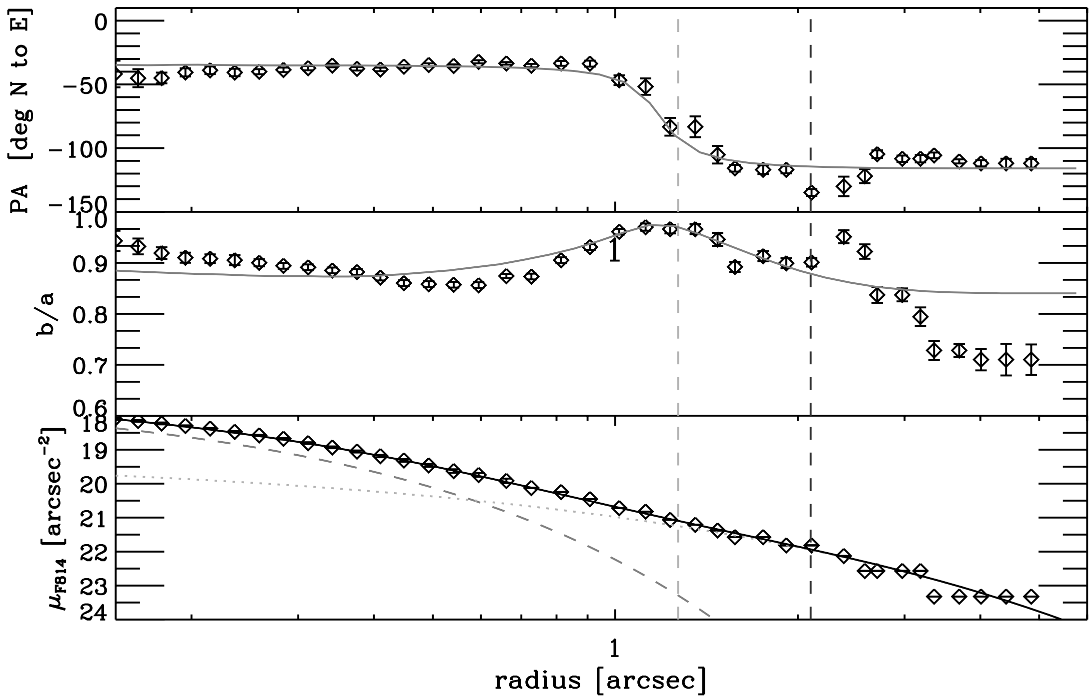

FIG. 2.—Results for isophotal fit with IRAF `ellipse`. *Top*: PA vs. radius. *Middle*: Axis ratio vs. radius. The vertical lines show the location of the inner and outer Einstein rings that were masked out during the fitting process. We also overlay in the top and middle panels as a gray solid line the `ellipse` output performed on the best-fit GALFIT two-dimensional brightness distribution. *Bottom*: Best-fit Sérsic profiles obtained with GALFIT. The formal error bars on the surface brightness profile are smaller than the data points. [*See the electronic edition of the Journal for a color version of this figure.*]

The addition of a second component is needed to provide a good fit in the center and to reproduce the isophotal twist in the outer regions. To reduce the effect of lensed features in the fit, we proceeded iteratively. We first masked the lensed features manually, then we performed GALFIT fits creating masks by 4 σ clipping. Two iterations were needed to achieve convergence.

The total magnitude of the lens obtained by summing the flux of the two Sérsic models is F814W $= 17.110 \pm 0.002$ after correction for Galactic extinction (Schlegel et al. 1998). The rest-frame V-band absolute magnitude is $M_V = -22.286 \pm 0.025$ using the K-correction of Treu et al. (2006). The errors are dominated by systematic uncertainties on the K-correction term. The most concentrated Sérsic component c_1 dominates at the center and accounts for about 17.5% of the total lens flux. The effective radius of c_1 is about 0.4″, whereas that of c_2 is $\sim$3″ with about 10% relative accuracy. Similarly, the Sérsic indices are $n_{c_1} \simeq 1.23$ and $n_{c_2} \simeq 1.75$.

To measure the one-dimensional light profile of the lens galaxy, we used the IRAF task `ellipse`. Figure 2 shows the radial change of ellipticity and position angle of the light distribution. There is a clear indication of a sharp change in position angle and ellipticity between 1″ and 2″. This isophotal twist is well captured by the double Sérsic profile fit, which requires different position angles (PAs) for the two components. Therefore, we conclude that the lens galaxy is made of two misaligned components, having similar surface brightness at radius $\sim$0.6″.

For comparison, a single-component Sérsic fit yields $n \simeq 3.73$, consistent with the typical light profiles of massive early-type galaxies. The effective radius of the composite surface brightness distribution is found to be $R_{\rm eff} = 2.02'' \pm 0.10'' \simeq 7.29 \pm 0.37\ h_{70}^{-1}$ kpc, where we assumed a typical relative uncertainty of about 5% as discussed in Treu et al. (2006). It is also consistent with an independent measurement reported by Bolton et al. (2008), who considered de Vaucouleurs surface brightness distributions ($n \equiv 4$ by construction). Note that we use the same convention for all characteristic radii reported throughout. For elliptical distributions radii are expressed at the intermediate radius [i.e., the geometric mean radius $r = (ab)^{1/2}$].

In addition, the stellar velocity dispersion $\sigma_{\rm ap} = 263 \pm 21$ km s^{-1} was measured with SDSS spectroscopy within a 3″ diameter fiber. We convert this velocity dispersion $\sigma_{\rm ap}$ into the fiducial velocity $\sigma_{v,*}$ that enters fundamental plane analyses and measured in an aperture of size $R_{\rm eff}/8$ using the relation $\sigma_{v,*}/\sigma_{\rm ap} = (R_{\rm eff}/8/R_{\rm ap})^{-0.04} \simeq 1.08$ (see Treu et al. 2006 and references therein).

Based on photometric redshifts available online on the SDSS Web site (Oyaizu et al. 2008), we note that the lens galaxy is the brightest galaxy in its neighborhood. Another bright galaxy about 40″ southwest of SDSS J0946+1006 exhibits perturbed isophotes (an extended plume), suggesting that it may have flown by recently and might end up merging onto the lens galaxy. Its photometric redshift is $z_{\rm phot} = 0.20 \pm 0.04$, consistent with the redshift of SDSS J0946+1006. The extended envelope captured by the double Sérsic component fit also supports the recent flyby hypothesis (e.g., Bell et al. 2006).

2.3. *Lensed Structures*

Two concentric partial ring–like structures are clearly seen at radii $1.43'' \pm 0.01''$ and $2.07'' \pm 0.02''$ from the center of the lens galaxy (Fig. 1). Such a peculiar lensing configuration, with widely different image separations of nearly concentric multiple-image systems, implies that the rings come from two sources at different redshift, the innermost (ring 1) corresponding to the nearest background source 1 and the outermost (ring 2) being significantly farther away along the optical axis.

Ring 1 has a typical cusp configuration with three merging conjugate images and a counterimage on the opposite side of the lens and closer to the center than the large cusp "arc." This constrains the orientation of the lens potential major axis to pass almost through the middle of both arcs. Ring 1 is among the brightest ones to have been discovered in the SLACS Survey (for the latest compilation see Bolton et al. 2008). The observed F814W magnitude is $m_1 = 19.784 \pm 0.006$ (extinction corrected). The error bar includes only statistical uncertainties. An additional systematic error of order $\lesssim 0.1$ mag is likely present due to uncertainties in the lens galaxy subtraction (Marshall et al. 2007).

Ring 2 presents a nearly symmetrical Einstein cross configuration (with a faint bridge between the north and west images), implying that the source must lie very close to the optical axis. The observed F814W magnitude is $m_2 = 23.68 \pm 0.09$, making it about 36 times fainter than ring 1. As for ring 1, the error bar includes only statistical uncertainties.

No evidence of ring 2 is present in the SDSS spectrum. This can be explained by the low peak surface brightness of ring 2 ($\sim$23 mag arcsec^{-2}) and less importantly by the diameter of the second ring being slightly larger than the 3″ SDSS fiber (although for a successful redshift measurement in a similar case see Bolton et al. 2006b). Deeper long-slit spectroscopy was obtained at Keck Observatory with the Low Resolution Imager Spectrograph (LRIS) instrument on 2006 December 22–23, the total integration time being about 9 hr. The goal was twofold: (1) obtain the redshift of ring 2 and (2) measure the stellar velocity dispersion profile of the main lens. The latter aspect will be presented elsewhere. Despite the large integration time, we could not measure the source redshift z_{s2} due to a lack of emission lines in the range [3500, 8600 Å] that do not belong to ring 1. Since ring 2 is detected in the ACS F814W filter, we can set an upper limit on its redshift $z_{s2} < 6.9$ by requiring that the Lyman break be at shorter wavelengths than the red cutoff of the filter.

3. LENS MODELING

3.1. *Model Definition*

This section describes our adopted strategy to model this exceptional lens system. We begin with a simplifying assumption. Although the gravitational potential arises from both a stellar and a dark matter component, a single power-law model for the total density profile turns out to be a good description of SLACS lenses (Koopmans et al. 2006). Therefore, we assume the total convergence for a source at redshift z_s to be of the form

$$\kappa(\boldsymbol{r}, z_s) = \frac{b_\infty^{\gamma'-1}}{2}\left(x^2 + y^2/q^2\right)^{(1-\gamma')/2}\frac{D_{\rm ls}}{D_{\rm os}}, \qquad (1)$$

with four free parameters: the overall normalization b, the logarithmic slope of the density profile γ', the axis ratio q, and position angle PA_0 (omitted in eq. [1] for simplicity) of iso-κ ellipses. The familiar case of the singular isothermal sphere is that corresponding to a slope $\gamma' = 2$ and $q = 1$. In this case b_∞ relates to the velocity dispersion of the isothermal profile by $b_\infty = 4\pi(\sigma_{\rm SIE}/c)^2 = (\sigma_{\rm SIE}/186.2\ \mathrm{km\ s^{-1}})^2$ arcsec. Note that $\sigma_{\rm SIE}$ is nothing but a way of redefining the normalization of the convergence profile and does not necessarily correspond in a straightforward sense to the velocity dispersion of stars in the lens galaxy. In general, for every combination of model parameters, the stellar velocity dispersion of a specified tracer embedded in the potential can be computed by solving the Jeans equation and will be a function of radius and observational effects such as aperture and seeing.

No assumptions are made about the orientation of the position angle PA_0 of the lens potential. In addition, we allow for external shear with modulus $\gamma_{\rm ext}$ and position angle $\mathrm{PA}_{\rm ext}$. For a multiple source plane system, it is necessary to define a lens plane from which the external shear comes since shear has to be scaled by the appropriate $D_{\rm ls}/D_{\rm os}$ term for each source plane. For simplicity we assume that the global effect of external perturbations comes from the same lens plane $z_l = 0.222$. We expect a strong degeneracy between internal ellipticity and external shear but include this extra degree of freedom in the model to account for any putative twist of isopotentials, as suggested by the observed isophotal twist in the lens galaxy surface brightness. Note also that the need of being able to handle two distinct source planes led us to the somewhat unusual definition of b_∞ in equation (1). With this convention, $(b_\infty\sqrt{q})^{\gamma'-1}D_{\rm ls}/D_{\rm os}$ is the quantity closest to the $b_{\rm SIE}$ (or $R_{\rm Ein}$) parameter used in other SLACS papers (Koopmans et al. 2006; Bolton et al. 2008). Note also that the center of mass is assumed to match exactly the lens galaxy center of light. The unknown redshift of source 2 is also treated as a free parameter, for which we assign a uniform $1_{s2} \leq 6.9$ prior. Altogether, we use seven free parameters to characterize the potential of SDSS J0946+1006: b_∞, γ', q, PA_0, $\gamma_{\rm ext}$, $\mathrm{PA}_{\rm ext}$, and z_{s2}.

In this section and the next, we neglect the extra focusing effect of ring 1 acting as a lens on ring 2, leaving the discussion of this perturber for § 5.

3.2. *Methods*

We consider three strategies for studying gravitational lens systems with spatially resolved multiple images.

The first one consists of identifying conjugate bright spots in the multiple images and minimizing the distance of conjugate points in the source plane. This approach is statistically conservative in the sense that it only takes partial advantage of the large amount of information present in the deep *HST* data. However, it has the benefit of being robust and relatively insensitive to the details of the source morphology, as well as other concerns that affect different alternative techniques in the case.

The second approach is the linear source inversion and parametric potential fitting method described by Warren & Dye (2003), Treu & Koopmans (2004), Koopmans (2005), and Suyu et al. (2006). A strong advantage of this method is that it takes fully into account the amount of information contained in each pixel. Although this method is robust, there are many degrees of freedom to model the intrinsic source surface brightness distribution, and thus some form of regularization is needed to avoid fitting the noise as described in the references above.

The third method (e.g., Marshall et al. 2007; Bolton et al. 2007, 2008) describes the source as one or several components parameterized with elliptical surface brightness profiles (usually Sérsic). In general, this method provides good fits to the data, as long as not too many such components are needed to represent the source, and directly provides physically meaningful parameters for the source. For high signal-to-noise ratio images of complex lensed features the dimensionality of the problem may increase very fast.

In the case of a multiple source plane system, two difficulties arise when using the second and third techniques: (1) Our current pixelized method does not handle multiple source planes (for recent progress along this line see, e.g., Dye et al. 2007). (2) The statistical weight given to each of the partial rings depends essentially on their relative brightness. Since ring 1 is 36 times brighter than ring 2, it completely dominates the fit. This has the unwanted side effect that a physically uninteresting morphological mismatch of the inner ring, due, for example, to poor modeling of the source or of the PSF, overwhelms any mismatch in the physically important *image separation* of the outer ring.

The goal of the present analysis is to confirm that SDSS J0946+1006 is the first example of a galaxy-scale double source plane

TABLE 1
Summary of Pixel Coordinates Used for Lens Modeling

Knot	Image 1	Image 2	Image 3	Image 4
S1a	0.34, −1.50	−0.94, 0.68	1.52, 0.19	...
S1b	...	−1.16, 0.22	1.44, 0.88	...
S1c	−0.43, −1.42	−1.10, 0.67	1.23, 0.88	...
S1d	−0.14, −1.68	−0.57, 0.96	...	...
S2	−1.51, −1.78	1.56, −1.19	1.55, 1.65	−1.34, 1.32

Notes.—Positions (x, y) of each multiple knot are expressed in arcseconds (typical rms error 0.03″) relative to the lens galaxy surface brightness peak (got from GALFIT modeling; see § 2.2). The frame PA is 161.348° relative to north.

system and illustrate what kind of information can be inferred from such a configuration. After experimenting with all three techniques, and in light of the difficulties described above, we decided to focus on the more straightforward conjugate points modeling technique, using the other techniques to aid in our modeling.

In practice, the modeling technique adopted here is similar to the one used by Gavazzi et al. (2003). The merging cusp nature of ring 1 makes the identification of quadruply imaged spots hazardous along the elongated arc, but identifications are much easier between the opposite counterimage and the elongated arc. The identification of the brightness peak S2 in ring 2 is obvious. To guide the identification process, we also used fits based on the pixelized source inversion. We ended up having four spots identified in ring 1, two of them having three clear conjugations (S1a, S1c), whereas the other two have only two (S1b, S1d). One single bright spot in ring 2 is imaged four times. The typical rms error made on the location of spots is estimated to be 0.03″. Table 1 summarizes the coordinates of matched points in the same frame as Figure 1. For each knot S1a, S1b, S1c, S1d, and S2, multiple images with positive parity have an odd labeling number. To guide the fitting procedure, we also demand the image parity to be preserved by the model. Therefore, taking into account the unknown position of these spots in the source plane, we end up having 18 constraints (see Gavazzi et al. 2003), whereas the considered model has seven free parameters. Hence, the optimization problem has 11 degrees of freedom.

4. MODELING RESULTS

The optimization process and the exploration of the parameter space were performed by sampling the posterior probability distribution function with Monte Carlo Markov Chains (MCMC). We assumed flat priors. Table 2 summarizes the results ("best-fit" values are defined as the median value of the marginalized PDF) and their corresponding 68% CL uncertainties after marginalizing the posterior over all the other parameters. The best-fit model yields a $\chi^2/\mathrm{dof} = 13.2/11 \simeq 1.20$, which is statistically reasonable.[10]

The results of the best-fit model inferred from the conjugation of bright spots are shown in Figure 3, where we used the pixelized source inversion technique to illustrate the quality of the fit and the reliability of the conjugation method. Although the surface brightnesses of rings 1 and 2 identified by separate annuli in the image plane are inverted separately, model predictions in the image plane are recombined for convenience. The two source planes $z_{s1} = 0.609$ and $z_{s2} \simeq 5$ are also shown.

As expected, there is a degeneracy between external shear and ellipticity of the total mass distribution and the modeling, suggesting that the major axis of the potential and the external shear differ by $\mathrm{PA}_0 - \mathrm{PA}_{\mathrm{ext}} = 20^{+12}_{-16}$ deg, that is, they are aligned within $\sim 1.2\,\sigma$. The orientation of external shear is in agreement with the orientation of stars out to $r \lesssim 1''$, which is about −36°. The orientation of the internal quadruple (lens ellipticity) and that of stars are misaligned by ∼24°. Likewise, the axis ratio of the light distribution over this radial range is $0.85 \lesssim b/a \lesssim 0.93$, again consistent with our lens model.

[10] A χ^2 distribution with 11 degrees of freedom gives a probability of 28% that the χ^2 value will be greater than 13.2.

TABLE 2
Best-Fit Model Parameters for SDSS J0946+1006 Using a Single Lens Plane

Parameter	Value
b_∞ (arcsec)	2.54 ± 0.09
γ'	2.00 ± 0.03
Axis ratio q	$0.869^{+0.017}_{-0.013}$
PA_0	$-11.8^{+7.0}_{-8.9}$
γ_{ext}	$0.067^{+0.010}_{-0.007}$
$\mathrm{PA}_{\mathrm{ext}}$	$-31.5^{+6.9}_{-4.8}$
z_{s2}	$5.30^{+1.03}_{-1.00}$
σ_{SIE} (km s^{-1})	$287.0^{+5.1}_{-5.3}$
"Unlensed" apparent $\mathrm{F814}_{s1}$ (mag)	22.76 ± 0.02 ± 0.10
"Unlensed" absolute V_{s1} (mag)	−19.79 ± 0.05 ± 0.10
"Unlensed" apparent $\mathrm{F814}_{s2}$ (mag)	27.01 ± 0.09 ± 0.10

Notes.—Best-fit model parameters and 68.4% confidence limits. Errors on magnitudes distinguish statistical (first) and systematic from lens light subtraction (second). Angles are in degrees oriented from north to east.

The lens modeling also puts interesting constraints on the redshift of source 2: $z_{s2} = 5.3 \pm 1.0$. The accuracy is relatively low because of the saturation of the $D_{\mathrm{ls}}/D_{\mathrm{os}}(z_s)$ curve when $z_s \to \infty$. The top panel of Figure 4 shows a mild correlation between z_{s2} and the slope of the density profile γ'. This is expected since the steeper the density profile that fits the inner ring, the less mass is enclosed between the two rings, and hence the farther away must be the outer source.

In spite of the complexity of the azimuthal properties of the lens potential, our modeling yielded stable and well-localized constraints on the normalization and slope of the radial total density profile. The bottom panel of Figure 4 shows the confidence regions for the slope γ' and the equivalent velocity dispersion σ_{SIE}. First, we find a total density profile very close to isothermal with a slope $\gamma' = 2.00 \pm 0.03$. The corresponding SIE velocity dispersion is $\sigma_{\mathrm{SIE}} = 287.0 \pm 5.2$ km s^{-1}. In order to compare these results with SDSS spectroscopy, one needs to solve the spherical Jeans equation taking into account observational effects (SDSS fiber aperture, seeing) and the surface density of dynamical tracers (radial distribution of stars in the lens galaxy) measured in § 2.2. Here we assume an isotropic pressure tensor. A general description of the method can be found in Koopmans (2006). Figure 5 shows the aperture velocity dispersion that would be measured with SDSS spectroscopic fibers when the density profile is normalized to fit the first ring alone. It shows that slopes close to isothermal ($\gamma' \simeq 2$) predict velocity dispersions close to SDSS spectroscopic velocity dispersion, which gives strong support to our double source plane lensing-only analysis. Such a similarity is consistent with the results of previous SLACS studies (Treu et al. 2006; Koopmans et al. 2006). We note that the accuracy reached on both the slope and the velocity dispersion based on lensing constraints alone is better than that afforded by kinematical measurements at the same redshift, although the two methods are complementary in their systematic errors and degeneracies (see discussion in, e.g., Treu & Koopmans 2002).

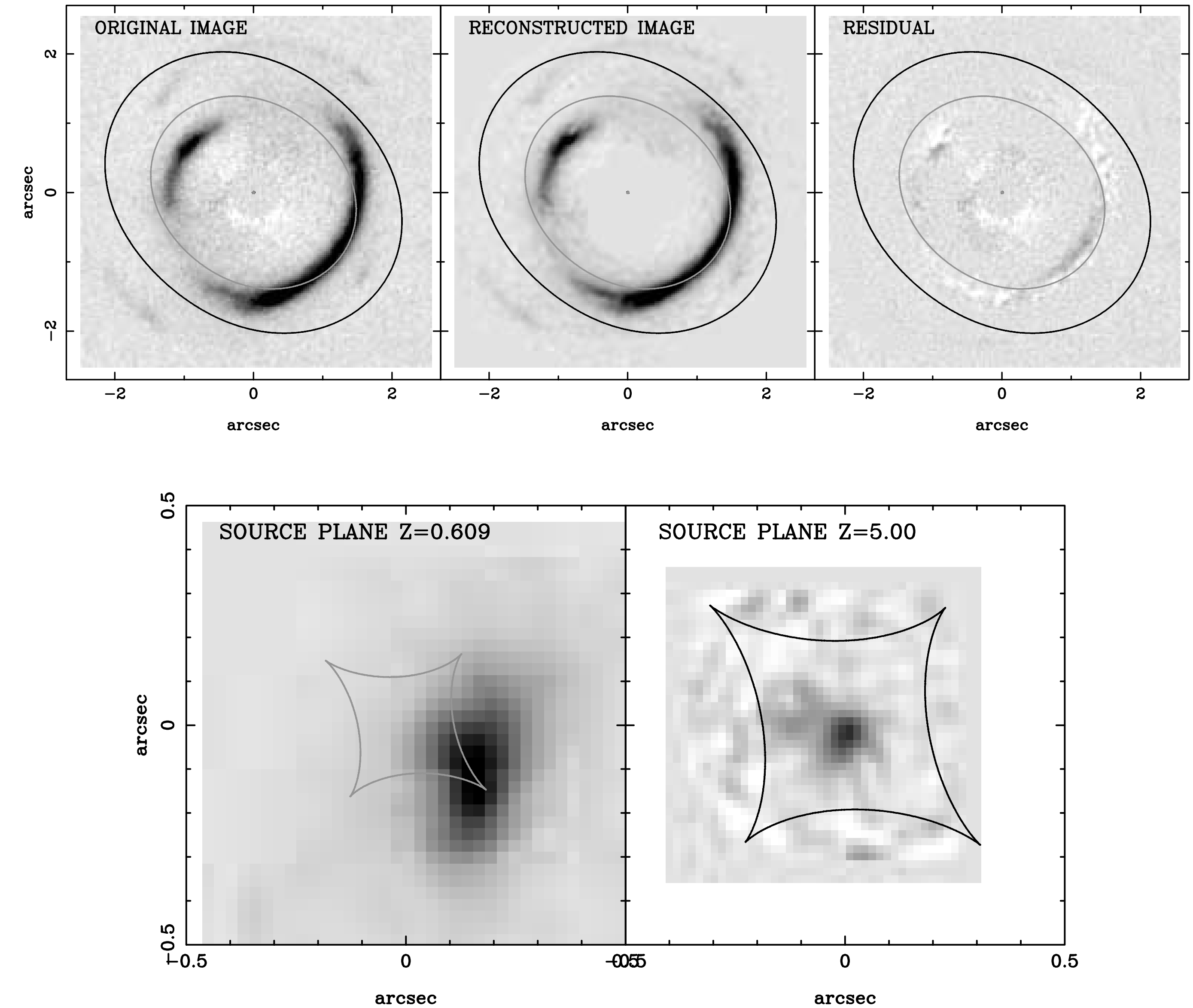

FIG. 3.—Best-fit single lens plane model for the lens SDSS J0946+1006. The model parameters were found using the identification of conjugate bright knots, but the quality of the model is illustrated with a pixelized source inversion technique. *Top left*: Observation with the lens light profile subtracted off. *Top middle and right*: Model prediction in the image plane and associated residuals. The model also predicts the light distribution in the source planes z_{s1} and z_{s2} (*bottom left and right, respectively*). Note a different color stretching for source plane 2 (factor of 6) in the latter case. Critical and caustic lines corresponding to the two source planes are overlaid (smaller for $z_{s1} = 0.609$ and wider for $z_{s2} = 5$). [*See the electronic edition of the Journal for a color version of this figure.*]

4.1. *Budget of Mass and Light in SDSS J0946+1006*

The tight constraints on the projected mass profile between the two Einstein radii can be compared to the light distribution inferred in § 2.2. In particular, the total projected *V*-band mass-to-light ratio within the effective radius $R_{\rm eff} \simeq 7.29\ h_{70}^{-1}$ kpc is $M/L_V = 11.54 \pm 0.51\ h_{70}\ (M/L_V)_\odot$ [corresponding to a total projected mass $(4.90 \pm 0.13) \times 10^{11}\ h_{70}^{-1}\ M_\odot$]. The logarithmic slope of the projected enclosed total mass profile is $3 - \gamma' = 1.00 \pm 0.03$, while the slope of the cumulative luminosity profile close to the effective radius is $d \log L(<r)/d \log r = 0.62$ with much smaller uncertainty. Therefore, the projected mass-to-light ratio profile increases with radius as $r^{0.38 \pm 0.03}$ around $R_{\rm eff}$ with high statistical significance.

We now compare these values to the stellar mass content in the effective radius using the typical mass-to-light ratio of stellar populations in massive galaxies at that redshift, $M_*/L_V \simeq 3.14 \pm 0.32\ h_{70}\ (M/L_V)_\odot$ (Gavazzi et al. 2007), and ~30% intrinsic scatter about this value (due to, e.g., age-metallicity effects) as found in the local universe (Gerhard et al. 2001; Trujillo et al. 2004). This leads to a fraction of projected mass in the form of dark matter within the effective radius $f_{\rm DM,2D}(<R_{\rm eff}) \simeq 73\% \pm 9\%$, which is about twice as high as the average value found by Gavazzi et al. (2007) and Koopmans et al. (2006), thus making SDSS J0946+1006 a particularly dark matter–rich system.

5. EXPLOITING THE DOUBLE SOURCE PLANE: BEYOND THE LENS MASS PROPERTIES

In this section we address two particular applications afforded by the double source plane nature of SDSS J0946+1006. First, in § 5.1 we discuss whether this particular system gives interesting constraints on cosmological parameters. Then, in § 5.2 we present a compound double lens plane mass model and use it to constrain the total mass of ring 1. This provides a new (and perhaps unique) way to obtain total masses of such compact and faint

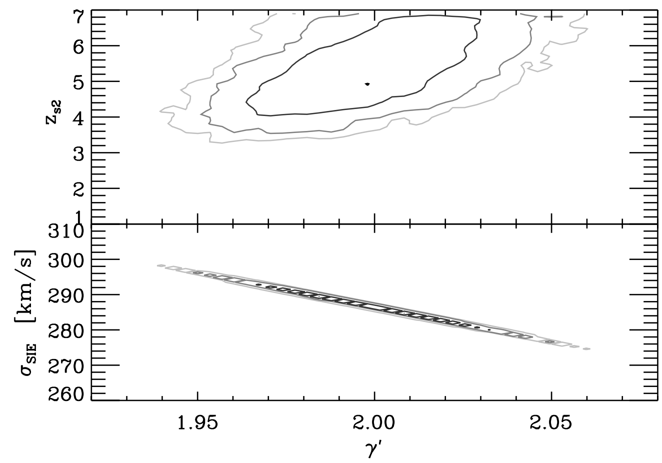

FIG. 4.—*Top*: 68.3%, 95.4%, and 99.3% CL contours for model parameters slope of the density profile γ' and source 2 redshift z_{s2}. *Bottom*: Same as the top panel, but for the slope γ' and the lens equivalent velocity dispersion [defined as $186.2(b_\infty q^{1/2}/1'')^{1/2}$ km s^{-1}]. [*See the electronic edition of the Journal for a color version of this figure.*]

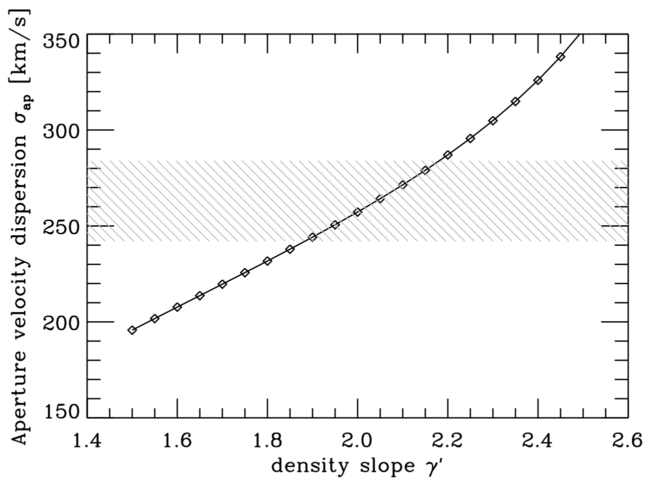

FIG. 5.—Predicted stellar aperture velocity dispersion $\sigma_{\rm ap}$ as it would be measured with SDSS spectroscopic settings as a function of the slope of the density profile. The normalization of density profile is fixed to be consistent with the Einstein radius of ring 1. The shaded area is the 1 σ SDSS measurement uncertainty. It shows a remarkable agreement between the double source plane analysis and the coupling of kinematical+source 1 plane data, both favoring nearly isothermal slopes. Note that $\sigma_{\rm ap}$ and $\sigma_{\rm SIE}$ do not need to be identical. [*See the electronic edition of the Journal for a color version of this figure.*]

objects. Thus, in combination with the magnifying power of the main lens, this application appears to be a promising way to shed light on the nature of faint blue compact galaxies (e.g., Marshall et al. 2007). In § 5.3 we discuss the prospects of doing cosmography with samples of double source plane lenses, taking into account the lensing effects of the inner ring on the outer ring.

5.1. *An Ideal Optical Bench for Cosmography?*

Can a double source plane lens be used to constrain global cosmological parameters like Ω_m or Ω_Λ? In principle, this can be done because lensing efficiency depends on the ratio of angular diameter distances to the source $D_{\rm os}$ and between the lens and the source $D_{\rm ls}$, as well as the projected surface mass density $\Sigma(\boldsymbol{\theta})$ in the lens plane. In formulae, writing the lens potential experienced by light rays coming from a source plane as redshift z_s as

$$\psi(\boldsymbol{\theta}, z_s) = \frac{4G}{c^2}\frac{D_{\rm ol}D_{\rm ls}}{D_{\rm os}}\int d^2\boldsymbol{\theta}\,\Sigma(\boldsymbol{\theta}')\ln|\boldsymbol{\theta}-\boldsymbol{\theta}'| \qquad (2)$$

$$\equiv \psi_0(\boldsymbol{\theta})\frac{D_{\rm ls}}{D_{\rm os}}, \qquad (3)$$

and considering two images at positions $\boldsymbol{\theta}_1$ and $\boldsymbol{\theta}_2$ coming from source planes at redshift z_{s1} and z_{s2}, one can measure the ratio of distance ratios $\eta \equiv (D_{\rm ls}/D_{\rm os})_{z_{s2}}/(D_{\rm ls}/D_{\rm os})_{z_{s1}}$ directly from the properties of the multiple images, given assumptions on the potential $\psi_0(\boldsymbol{\theta})$ and its derivatives defining the deflection, convergence, and shear at the positions of the images.

Applications of this method to clusters of galaxies with several multiply imaged systems at different source redshifts, assuming simple parametric models for the clusters, seem to favor $\Omega_m < 0.5$ cosmologies (Golse et al. 2002; Soucail et al. 2004). However, unknown systematics lurks under the cluster substructure, which can introduce significant local perturbations of $\psi_0(\boldsymbol{\theta})$. In principle, at least judging qualitatively from the smoothness of the isophotes and the smoothness of galaxy-scale Einstein rings, one could hope that massive elliptical galaxies are less prone to this sort of systematic because source size is large compared to the substructure angular scale.

In the previous section we constrained z_{s2} for the given ΛCDM concordance cosmology. Here we reparameterize the problem using η itself as a free parameter to constrain the change in lensing efficiency between the two source planes. The left panel of Figure 6 shows the joint constraints on the two parameters γ' and η. A first consequence of this more general parameterization is that, by allowing a broader range of values for η (i.e., allowing more freedom in the cosmological model), the uncertainties on the slope are significantly increased: we find $\gamma' = 2.07 \pm 0.06$. Steeper density profiles are now somewhat compensated by a relatively higher lensing efficiency for the second source plane. In other words, the tight constraints previously obtained on the slope of the density profile depend to some extent on the assumed cosmological model (i.e., assuming ΛCDM cosmology led to $\gamma' = 2.00 \pm 0.03$).

The right panel of Figure 6 shows $\eta(z_{s2})$ as a function of the second source redshift for two "extreme" flat cosmologies: $(\Omega_m, \Omega_\Lambda) = (0.3, 0.7)$ and $(\Omega_m, \Omega_\Lambda) = (1., 0.)$, intermediate

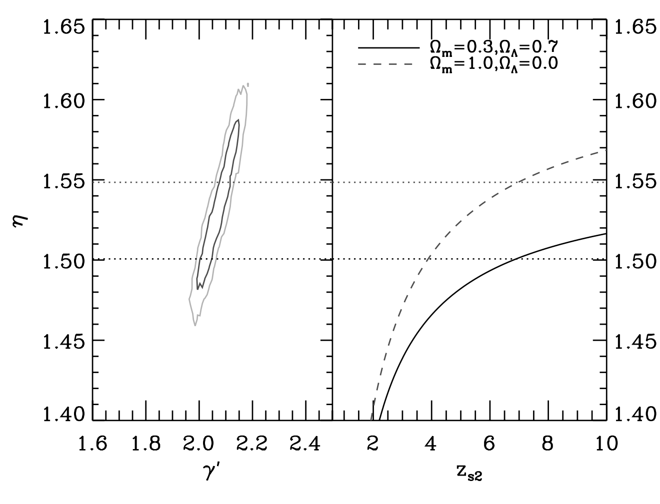

FIG. 6.—*Left*: Constraints on the logarithmic slope γ' and the ratio of distance ratios η. Contours enclose 68.3% and 95.4% of probability. *Right*: $\eta(z_{s2})$ as a function of z_{s2} for two flat cosmologies $(\Omega_m, \Omega_\Lambda) = (0.3, 0.7)$ (*black*) and $(\Omega_m, \Omega_\Lambda) = (1., 0.)$ (*gray*), which are two sensible "extreme" cases. The dotted horizontal lines illustrate the upper limits on η for these cosmologies given the assumption $z_{s2} \leq 6.9$ (see § 2.3). [*See the electronic edition of the Journal for a color version of this figure.*]

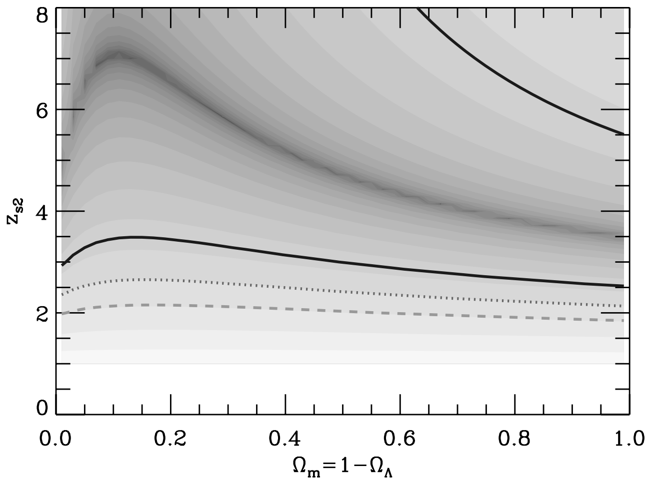

FIG. 7.—The 68.3%, 95.4%, and 99.3% CL contours in the redshift of source 2 and Ω_m parameter space assuming an isothermal density profile. This shows that even using strong priors on the density profile and for a given source redshift, only loose constraints can be inferred on cosmological parameters with a single double source plane system. [*See the electronic edition of the Journal for a color version of this figure.*]

cases lying in between. This shows that high values $\eta \gtrsim 1.57$ are not consistent with currently favored cosmologies. The upper limit on $\eta(z_{s2} = 6.9)$ is also shown for these two cases. This illustrates that very loose constraints can be obtained on cosmological parameters even if z_{s2} were known spectroscopically. Likewise, even assuming an isothermal slope of the density profile as motivated by joint lensing and dynamical analyses (Koopmans et al. 2006) does not drastically improve the constraints on η and consequently on cosmology as shown in Figure 7, even if z_{s2} could be measured with spectroscopic precision.

However, it is important to point out that the formal $\sim$3% relative uncertainty we get on η from our lens modeling strategy based on the identification of conjugate knots underestimates the potential accuracy of the method. Statistical errors would decrease by a factor of a few with a full modeling of the surface brightness distribution in the image plane. Unfortunately, the error budget would then be limited by additional systematic sources of uncertainty like extra convergence coming from large-scale structures along the line of sight with estimated standard deviation $\sigma_\kappa \gtrsim 0.02$ (Dalal et al. 2005) or due to a nontrivial environment in the main lens plane. Therefore, we conclude that it is unlikely that any cosmographic test based on the unique multiple Einstein ring system SDSS J0946+1006 will provide valuable information on cosmological parameters. The prospects of using large numbers of double source plane lenses are investigated in § 5.3.

5.2. *Source 1, Alias Lens 2*

Among the massive perturbers along the line of sight to source 2, the most prominent is probably the mass associated with source 1. Since the lens modeling predicts that both sources are located very close to the optical axis (the center of the lens; see bottom panels of Fig. 3), the light rays coming from source 2 to the observer will experience the potential of source 1 before that of the main lens. Figure 8 illustrates the complexity of the configuration, which adds some extra positive focusing for the second source plane. For the cosmological applications we mentioned above, this translates into a small but systematic source of bias. The bias introduced on the inferred mass profile of the main lens is small, so that the conclusions presented in § 4 are not significantly altered except for the estimate of z_{s2}.

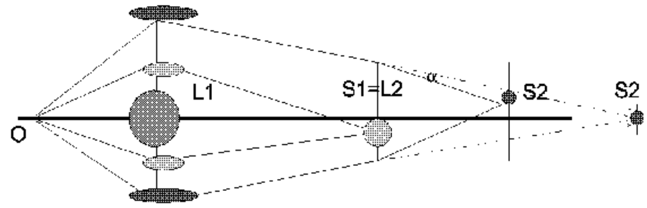

FIG. 8.—Sketch of the lensing optical bench with source 1 acting as a perturbing lens on source 2, which complicates the relation between redshifts, deflection angles, and angular distances. [*See the electronic edition of the Journal for a color version of this figure.*]

On the bright side, this lens configuration allows us to obtain some insight on the mass associated with ring 1 (also identified as "lens 2") provided that we now fully take into account the multiple lens plane nature of such lines of sight (e.g., Blandford & Narayan 1986; Schneider et al. 1992; Bartelmann 2003). This is the purpose of the present section, in which we fix the ΛCDM concordance cosmological model for simplicity.

To achieve this goal, we have to address the mass properties of the main lens at the same time as those of the first source 1. We reconsider the lens model of § 3 but add another mass component at redshift $z_{l2} = z_{s1} = 0.609$ in the form of a singular isothermal sphere with free equivalent velocity dispersion parameter $\sigma_{\mathrm{SIE},s1}$ and centered on the position of source 1. As in § 3, our uncertainty on the distance to source 2 is simply parameterized by its redshift z_{s2} in the context of a ΛCDM cosmological model.

In multiple lens plane theory, the relation between the angular position $\boldsymbol{\theta}_j$ of a light ray in the jth lens plane and the angular position in the $j = 1$ image plane is

$$\boldsymbol{\theta}_j(\boldsymbol{\theta}_1) = \boldsymbol{\theta}_1 - \sum_{i=1}^{j-1} \frac{D_{ij}}{D_j} \hat{\boldsymbol{\alpha}}(\boldsymbol{\theta}_i). \quad (4)$$

The last lens plane N can be identified with the source plane such that $\boldsymbol{\theta}_N = \boldsymbol{\beta}$. In equation (4), as compared to Bartelmann (2003), we did not consider the *reduced* deflection, which introduces an unnecessary extra D_{is}/D_s term in the sum. Likewise, the sign convention for the deflection is different than in Bartelmann (2003). Therefore, for two distinct positions $\boldsymbol{\theta}_1$ and $\boldsymbol{\theta}_2$ coming from two distinct source plane positions $\boldsymbol{\beta}_1$ and $\boldsymbol{\beta}_2$, respectively, we can write

$$\boldsymbol{\beta}_1 = \boldsymbol{\theta}_1 - \frac{D_{\mathrm{ls1}}}{D_{s1}} \hat{\boldsymbol{\alpha}}(\boldsymbol{\theta}_1), \quad (5)$$

$$\boldsymbol{\beta}_2 = \boldsymbol{\theta}_2 - \frac{D_{\mathrm{ls2}}}{D_{s2}} \hat{\boldsymbol{\alpha}}(\boldsymbol{\theta}_2) - \frac{D_{s1s2}}{D_{s2}} \hat{\boldsymbol{\alpha}}_{s1} \left[\boldsymbol{\theta}_2 - \frac{D_{\mathrm{ls1}}}{D_{s1}} \hat{\boldsymbol{\alpha}}(\boldsymbol{\theta}_2) - \boldsymbol{\beta}_1\right]. \quad (6)$$

In these equations, $\hat{\alpha}$ is the deflection produced by the main lensing galaxy (lying in the plane that also defines the image plane) and $\hat{\alpha}_{s1}$ is the perturbing deflection produced by source 1 (lens 2) onto source 2. Note that parameters like the center of source 1 enter the modeling scheme as both source and lens plane parameters. This is clearly visible in the brackets for the argument of $\hat{\alpha}_{s1}$ that contains $\boldsymbol{\beta}_1$, the position of source 1 in the source plane.

The constraints obtained on the equivalent velocity dispersion parameter of the main lens σ_{SIE} and that of source 1 $\sigma_{\mathrm{SIE},s1}$ are shown in the left panel of Figure 9. We clearly see two kinds of solutions: one (family I) has a high lens velocity dispersion (and slope $\gamma' \sim 1.96$, nearly isothermal) and little mass in source 1,

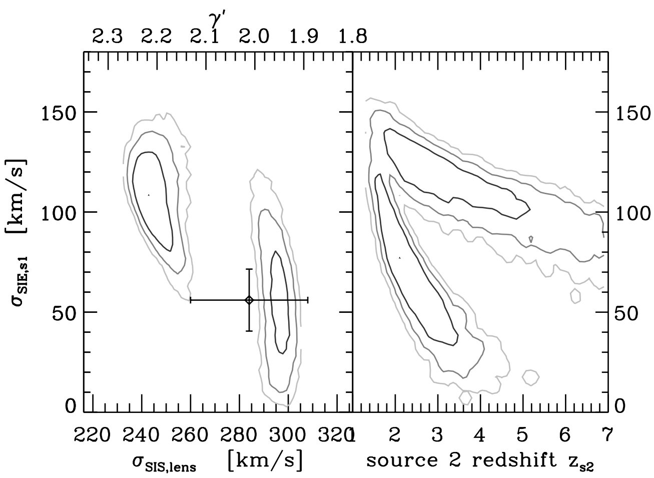

FIG. 9.—*Left*: Contours in parameter space of the velocity dispersion of the main lens $\sigma_{\rm SIE}$ and that of the first source $\sigma_{{\rm SIE},s1}$. Given the tight correlation $\sigma_{\rm SIE} \simeq (687 - 200.3\gamma')$ km s^{-1} found in § 4, the upper abscissa shows the correspondence with slope γ'. The kinematical SDSS estimate of $\sigma_{v,*}$ and the velocity dispersion of source 1 inferred from the Tully-Fisher relation (Moran et al. 2007) are overlaid as a point with error bar. *Right*: Contours in parameter space of the second source redshift z_{s2} and the velocity dispersion of the first source $\sigma_{{\rm SIE},s1}$. The recovered z_{s2} strongly depends on the mass enclosed in source 1. In both panels confidence levels mark the 68.3%, 95.4%, and 99.3% enclosed probability. [*See the electronic edition of the Journal for a color version of this figure.*]

whereas the other family (family II) has a lower main lens velocity dispersion and more mass in source 1. We measure ($\sigma_{\rm SIE}$, $\sigma_{{\rm SIE},s1}$) = ($295^{+3.5}_{-5.0}$, 56 ± 30) km s^{-1} for family I and ($\sigma_{\rm SIE}$, $\sigma_{{\rm SIE},s1}$) = ($247.3^{+8.5}_{-5.7}$, 104^{+21}_{-26}) km s^{-1} for family II. A pixelized source plane inversion for both of these best-fit models is shown in Figure 10. Family I models are shown in the top row and family II in the bottom row. Note the very complex systems of caustic and critical lines produced by this multiple lens plane system. It is difficult to favor either of these models based on a visual inspection, and either region on the parameter space has about the same statistical weight (fraction of MCMC samples). Uncertainties on recovered model parameters are summarized in Table 3.

The left panel of Figure 9 also shows the aperture-corrected SDSS-inferred velocity dispersion of the lens $\sigma_{v,*} = 284 \pm 24$ km s^{-1}, which seems to favor family I solutions, based on the earlier SLACS results of a general agreement between stellar velocity dispersion and $\sigma_{\rm SIE}$. In addition, we can get further external information on the mass of source 1, by extrapolating the Tully-Fisher relation found by Moran et al. (2007) at $z \sim 0.5$ for late-type galaxies. In the field, they found that at absolute magnitudes of $V \sim -19.7$, the maximum rotation velocity is $\log(2V_{\rm max}) = 2.2 \pm 0.1$. Assuming $V_{\rm max} \simeq \sqrt{2}\sigma_{\rm SIE}$, this translates into an estimate $\sigma_{{\rm SIE},s1} \simeq 59 \pm 13$ km s^{-1}. Another piece of information comes from weak-lensing results at intermediate redshift ($0.2 < z < 0.4$) by Hoekstra et al. (2005), who found that galaxies with magnitude $V - 5\log h \simeq -19$ have virial masses $M_{\rm vir} \simeq 1.50^{+0.99}_{-0.64} \times 10^{11}\, h_{70}^{-1}\, M_\odot$, which also corresponds to $\log(2V_{\rm max}) = 2.20 \pm 0.09$, in good agreement with Moran et al. (2007). These two arguments also seem to favor family I solutions, i.e., those with more mass in the main lens and less in source 1.

The right panel of Figure 9 shows the important degeneracy between the redshift of source 2 and the velocity dispersion of source 1. We can see that the more massive source 1, the lower z_{s2} must be. This demonstrates that any cosmographic test based on multiple source plane lens systems should carefully consider the mass in the foreground source as a significant perturbation on light rays coming from the most distant source. Adding a substantial amount of mass in source 1 significantly changes the inferred redshift of source 2 for either family I models, which yield $z_{s2} = 2.6^{+1.0}_{-0.7}$, or family II models, yielding $z_{s2} = 3.8^{+1.9}_{-1.5}$. Marginalizing over the whole posterior PDF gives $z_{s2} = 3.1^{+2.0}_{-1.0}$.

5.3. *Future Outlook: Cosmography with Many Double Source Plane Lenses*

In § 5.1 we explored the possibility of constraining cosmology with SDSS J0946+1006 and came to the conclusion that the errors are too large for this to be interesting. In § 5.2 we saw that the mass of the closest source must be taken into account as a perturbation along the double source plane optical bench. Here we attempt to address the possibility of using large numbers of such multiple lensing systems to probe the cosmology. Future space-based missions like *DUNE* or *JDEM* should provide us with tens of thousands of lenses, among which several tens would be double source plane systems. We also assume that redshifts will be available, from space- or ground-based spectroscopic follow-up.

First, we summarize the error budget expected for a typical double source plane system. As described before, the main quantity of interest is the ratio of distance ratios parameter $\eta \equiv (D_{\rm ls}/D_{\rm os})_2/(D_{\rm ls}/D_{\rm os})_1$, where source 2 is the farthest one. For simplicity, we assume that the main lens, the first source, and the second source are perfectly aligned onto the optical axis, resulting in two complete concentric rings of radius θ_1 and θ_2. The lens equation for each source plane reads

$$\beta_1 = \theta_1 - (D_{\rm ls}/D_{\rm os})_1 \alpha_{\rm tot}(\theta_1) = 0, \quad (7)$$

$$\beta_2 = \theta_2 - (D_{\rm ls}/D_{\rm os})_2 \alpha_{\rm tot}(\theta_2) = 0. \quad (8)$$

We consider again the general power-law surface mass distribution of equation (1) producing deflections α_1 and α_2 on source 1 and source 2 light rays. For source 2 we must add α_p, the *small* perturbing deflection[11] due to source 1 and experienced by source 2 only. Combining equations (7) and (8) gives

$$\eta = \left(\frac{\theta_2}{\theta_1}\right)^{\gamma'-1} \frac{1}{1 + (D_{s1s2}/D_{\rm ls2})(\alpha_P/\alpha_2)}. \quad (9)$$

This equation shows the importance of the perturbation. If one aims at constraining η with interesting accuracy (i.e., error smaller than 0.01), the small perturbing term in the denominator of second part on the right-hand side of equation (9) should be smaller than 0.01. Keeping in mind that for lensing potentials close to isothermal $\alpha \propto \sigma^2$, and that the typical velocity dispersion of the main lens is about $\sigma \simeq 250$ km s^{-1}, it is important to control and correct perturbing potentials with velocity dispersion as small as $\sigma_p = \sigma/10 \sim 30$ km s^{-1} for values $D_{s1s2}/D_{\rm ls2} \simeq 0.5$.

Next, differentiating equation (9) and writing $r \equiv \theta_2/\theta_1$, one can infer the fractional error on η:

$$\left(\frac{\delta_\eta}{\eta}\right)^2 = (\gamma'-1)^2\left(\frac{\delta_r}{r}\right)^2 + (\ln r)^2\delta_{\gamma'}^2 + \frac{4}{\left[1 + (D_{\rm ls2}/D_{s1s2})\left(\sigma^2/\sigma_P^2\right)\right]^2}\left(\frac{\delta_{\sigma_p}}{\sigma_p}\right)^2. \quad (10)$$

The first contribution is the relative measurement error on the ratio of Einstein radii, with typical values $0.001 \leq \delta_r/r \leq 0.03$

[11] We assume that the nonlinear coupling between lens planes can be neglected, i.e., the perturbation of source 1 is small compared to the deflection from the main lens on source 2 light rays: $\alpha_p \ll \alpha_2 \simeq \theta_2$.

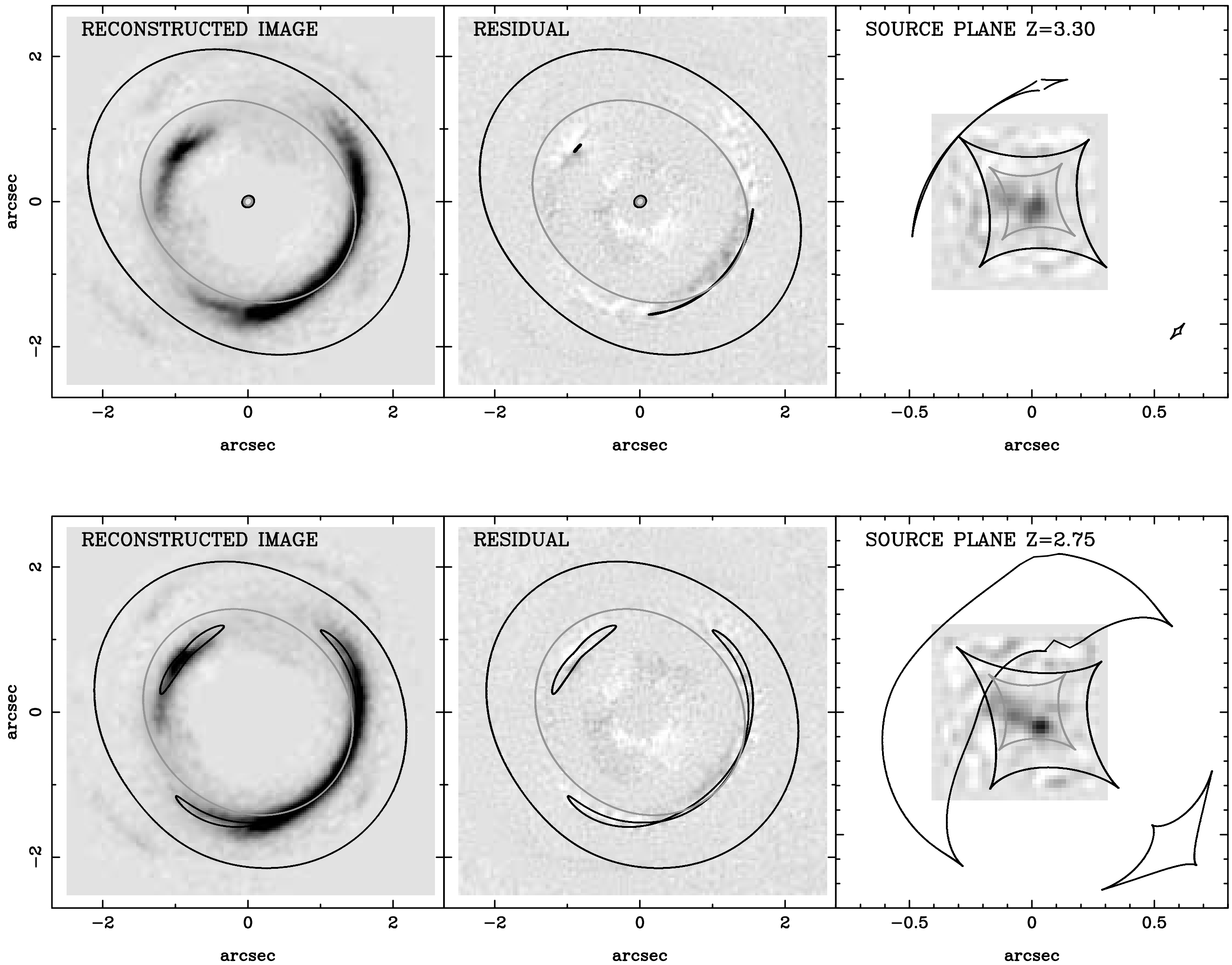

FIG. 10.—*Top*: Best-fit family I model image and source plane reconstructions. *Left to right*: Reconstructed image plane, residual (data minus model), and source 2 plane at redshift $z_{s2} = 3.30$. *Bottom*: Same as the top panels, but for the best-fit family II models (with $z_{s2} = 2.75$). Note the complex critical and caustic curves for the z_{s2} source plane due to the multiple lens plane configuration produced by source 1. For both models the reconstruction is satisfying and produces very few residuals. [*See the electronic edition of the Journal for a color version of this figure.*]

TABLE 3

Best-Fit Model Parameters for SDSS J0946+1006 Using a Compound Double Lens Plane

Parameter	Family I	Family II	Global
b_∞ (arcsec)	$2.65^{+0.07}_{-0.10}$	$1.91^{+0.07}_{-0.06}$	$1.98^{+0.69}_{-0.11}$
γ'	$1.96^{+0.03}_{-0.02}$	$2.23^{+0.03}_{-0.05}$	$2.18^{+0.07}_{-0.22}$
Axis ratio q	$0.889^{+0.057}_{-0.016}$	$0.816^{+0.129}_{-0.027}$	$0.879^{+0.067}_{-0.083}$
PA_0	$-15.9^{+9.5}_{-12.2}$	$-17.9^{+9.2}_{-17.3}$	$-17.0^{+9.3}_{-15.5}$
$\gamma_{\rm ext}$	$0.069^{+0.016}_{-0.009}$	$0.089^{+0.026}_{-0.012}$	$0.082^{+0.026}_{-0.016}$
$\mathrm{PA}_{\rm ext}$	$-27.6^{+6.1}_{-6.7}$	$-26.5^{+6.2}_{-6.7}$	$-27.0^{+6.2}_{-6.7}$
z_{s2}	$2.6^{+1.0}_{-0.7}$	$3.8^{+1.9}_{-1.5}$	$3.1^{+2.0}_{-1.0}$
$\sigma_{{\rm SIE},s1}$ (km s^{-1})	$56.6^{+30.3}_{-27.6}$	$108.9^{+18.0}_{-19.9}$	$94.0^{+26.7}_{-46.6}$
$\sigma_{\rm SIE}$ (km s^{-1})	295^{+3}_{-4}	246^{+7}_{-5}	254^{+43}_{-11}

Notes.—Best-fit model parameters and 68.4% confidence limits. Angles are in degrees oriented from north to east.

for deep space-based imaging. The second term captures our prior uncertainty on the slope of the density profile (for example, Koopmans et al. [2006] measured $\langle\gamma'\rangle \simeq 2.01$ and an intrinsic scatter $\delta_{\gamma'} \simeq 0.12$). Finally, the third term represents our prior knowledge of the mass of the perturber, which can be based, for example, on the Tully-Fisher relation. Moran et al. (2007) estimated $\delta_{\sigma_p}/\sigma_p \simeq 0.25$. Inserting those values into equation (10) and assuming a typical value of $r \simeq 1.5$, we find a relative uncertainty on $\delta_\eta/\eta \simeq 0.06$ for a single system. The error is dominated by model uncertainties on the slope of the density profile and the mass in source 1. In the case of SDSS J0946+1006, we achieve a similar accuracy when using the above priors on the slope and the velocity dispersion of source 1. In the following we use a conservative $\delta_\eta/\eta = 0.08$ fiducial value.

Having estimated the accuracy achievable on η for a single double source plane system, we focus on the cosmological meaning of η in a spatially flat universe dominated by dark matter (Ω_m) and dark energy ($\Omega_{\rm DE} = 1 - \Omega_m$) with equation-of-state parameter $w = p_{\rm DE}/\rho_{\rm DE}$. It is worth pointing out that the ratio of angular diameter distances is independent of the Hubble constant H_0.

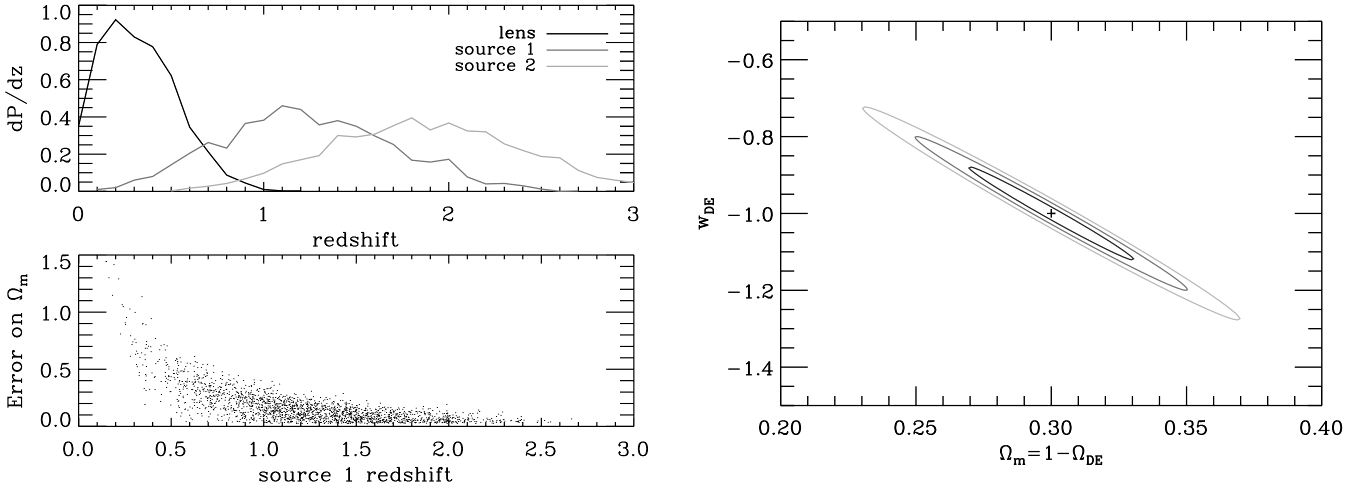

FIG. 11.—*Top left*: Redshift distribution for the lens, source 1, and source 2 used in the Monte Carlo simulation of mock double source plane lenses as they could be discovered in future space-based surveys. *Bottom left*: Individual error brought by each system on Ω_m as a function of the redshift of the first source. *Right*: 68.3%, 95.4%, and 99.3% CL contours on the matter density Ω_m and equation of state of dark energy $w = p/\rho$ obtained when combining 50 multiple source plane systems. [*See the electronic edition of the Journal for a color version of this figure*.]

The constraints on (Ω_m, w) are shown in the right panel of Figure 11. The error contours are obtained using a Fisher matrix formalism. We assumed a sample of 50 double source plane lenses, randomly produced using Monte Carlo simulations. The redshift distribution of lenses and sources used for the Monte Carlo simulations is shown in the top left panel of Figure 11. For the parent population of sources, it is based on recent COSMOS estimates (Leauthaud et al. 2007). The equivalent velocity dispersion of the lenses is assumed to be Gaussian with mean and standard deviation of 190 and 60 km s^{-1}, respectively. The Einstein radii for the first and second ring are constrained to be greater than 0.7″ and 1.0″, respectively.

The cosmological parameters Ω_m and w are recovered with a precision ±0.020 and ±0.080, respectively. We note that the sensitivity and the orientation of the degeneracy in this set of cosmological parameters are similar to those obtained with a Type Ia supernova experiment (see, e.g., Réfrégier et al. 2006 and references therein). The bottom left panel of Figure 11 demonstrates that the systems that contribute the most to constraining Ω_m are those with source 1 redshift $z_{s1} \gtrsim 1$ (a similar trend is seen for w). Lens redshifts larger than $\sim$0.5 are also more efficient configurations. This can easily be understood since the higher the redshifts of either lens, first or second source, the more sensitive distances are on cosmological parameters. Note that situations with very low redshift lenses but high-redshift sources 1 and 2 will result in a rapid saturation of the $D_{\rm ls}/D_{\rm os}$ for both sources 1 and 2, leading to values $\eta \simeq 1$ independent of cosmology. The sensitivity on cosmology is actually essentially driven by the redshift of the primary lens. Therefore, we conclude that SDSS J0946+1006 is not an optimal double source plane lens system for cosmographic purposes.

However, the prospects of doing cosmography with future samples of double source plane lenses are excellent, provided that systematic effects are controlled. The main source of systematic uncertainty that was ignored in the above calculations is the possibility of a change in the mean density slope as a function of lens redshift $\langle\gamma'\rangle = f(z_l)$ as present data seem to suggest that the dynamical properties of early-type galaxies have not changed much since $z \sim 1$. Koopmans et al. (2006) found $d\langle\gamma'\rangle/dz = 0.23 \pm 0.16$ over the redshift range [0.08, 1.01]. Progress needs to be made along this line to improve our knowledge of $\langle\gamma'\rangle = f(z_l)$, but a great advantage of double source plane systems over single ones is that combining stellar dynamics and lensing constraints from two source planes would be more efficient at "self-calibrating" the method than using single ones. In addition, a thorough lensing analysis aiming at carefully modeling the surface brightness of lensed structures will certainly help in controlling any such evolution trend of the density profile (see, e.g., Dye & Warren 2007).

6. SUMMARY AND CONCLUSIONS

In this paper we report the discovery of the first galaxy-scale double lensing event made of a foreground lens galaxy at redshift $z_l = 0.222$, a first source at redshift $z_{s1} = 0.609$ (ring 1) and a more distant source (ring 2) with unknown redshift, despite an attempt to measure its redshift with deep optical spectroscopy using LRIS on the Keck I Telescope. The detection of ring 2 in a single-orbit *HST* ACS F814W filter image sets an upper limit to its redshift $z_{s2} < 6.9$.

Modeling the geometry of the lensed features at different source planes, we determine the mass density profile of the lens galaxy, which is found to be close to isothermal. The best-fit lens model predicts a stellar velocity dispersion in very good agreement with that measured from SDSS spectroscopy. The model requires a relatively large amount of dark matter inside the effective radius $f_{\rm DM,2D}(<R_{\rm eff}) \simeq 73\% \pm 9\%$ [corresponding to a projected total mass-to-light ratio $M/L_V = 11.54 \pm 0.13\ h_{70}\ (M/L_V)_\odot$], assuming the stellar mass-to-light ratio measured in Gavazzi et al. (2007). Along with the complex isophotes of the lens galaxy and the presence of several other (less luminous) galaxies at similar photometric redshifts, the high dark matter fraction suggests that the lens may be the central galaxy of a group-scale halo. The high precision of this measurement, far superior to that attainable from single multiply imaged systems, demonstrates that double source plane lenses are extremely valuable tools to study the mass profile of galaxies and groups.

In order to constrain the redshift of ring 2 and assess the feasibility of determining cosmological parameters using double source plane lenses, we constructed multiple lens plane mass models. In that case the lensing effect of ring 1 on ring 2 is taken into account and modeled as a singular isothermal sphere. Although the extra mass component adds additional uncertainty to the derived z_{s2} and cosmological parameters, it provides a unique way to determine the total mass of the intermediate galaxy (the inner ring). Discarding the family II range of solutions (disfavored by kinematics of stars on the main lens galaxy), the two lens plane mass model results can be summarized as follows:

1. The redshift of ring 2 is found to be $z_{s2} = 2.6^{+1.0}_{-0.7}$. This is a genuine prediction that can be tested with the help of deep *HST* images at shorter wavelengths, using the dropout technique.

2. No interesting constraints on cosmological parameters can be obtained from the lensing analysis of the system SDSS J0946+1006, due to the unknown redshift of ring 2, the overall degeneracy of cosmography with the slope of the mass density profile between the rings, the degeneracy with the mass of the inner ring, and the suboptimal combination of lens and source redshifts.

3. The velocity dispersion of ring 1 is found to be $\sigma_{\rm SIE} = 56 \pm 30$ km s^{-1}, in good agreement with the value expected based on the extrapolation of the Tully-Fisher relation at this redshift (Moran et al. 2007) and on weak-lensing measurements (Hoekstra et al. 2005). Given that lensing cross section increases with the fourth power of the velocity dispersion, individual lenses in this mass range are expected to be very rare. In addition, it is observationally more difficult to identify lensed background structures embedded in foreground late-type galaxies with small Einstein radius (for both imaging and spectroscopic lens searches). Thus, double source plane lenses, also seen as double lens plane systems, may be effective at determining the lensing mass of small distant galaxies, complementing detailed photometric studies (Marshall et al. 2007) and kinematic studies with integral field spectrographs on large ground-based telescopes with adaptive optics.

Future planned space missions like *JDEM* or *DUNE* are expected to deliver several tens of thousands of single source plane lenses (Aldering et al. 2004; Marshall et al. 2005; Réfrégier et al. 2006) and several tens of double source plane lens galaxies. Given the great utility of multiple source plane lenses as tools to study distant galaxies and the relatively small number of expected systems, we argue that the necessary effort of spectroscopic follow-up would be easily affordable and well motivated.

In addition, a relatively large sample of double source plane galaxy-scale gravitational lenses will be a practical tool for cosmography. As an example, we calculated the constraints on Ω_m and the equation of state of dark energy $w = p_{\rm DE}/\rho_{\rm DE}$ that can be obtained from a sample of 50 double source plane lenses, assuming that both source redshifts are known and are realistically distributed. Spectroscopic follow-up of such systems is also required to control systematic effects such as the change in the mean density profile slope as a function of the lens galaxy redshift. A careful analysis taking into account the uncertainty on the mass profile of the main lens and of the perturber shows that cosmological parameters can be measured with an accuracy of 10%, comparable to that obtained from the Hubble diagram of Type Ia supernovae.

The authors are thankful to the anonymous referee for several useful comments that greatly improved the clarity and quality of the paper, especially regarding multiple lensing probabilities. This research is supported by NASA through *Hubble Space Telescope* programs SNAP-10174, GO-10494, SNAP-10587, GO-10798, and GO-10886. T. T. acknowledges support from the NSF through CAREER award NSF-0642621 and the Sloan Foundation through a Sloan Research Fellowship. He is also supported by a Packard Fellowship. The work of L. A. M. was carried out at Jet Propulsion Laboratory, California Institute of Technology under a contract with NASA. L. V. E. K. is supported in part through an NWO-VIDI program subsidy (project number 639.042.505). He also acknowledges the continuing support by the European Community's Sixth Framework Marie Curie Research Training Network Programme, contract MRTN-CT-2004-505183 "ANGLES." P. J. M. acknowledges support from the Tabasgo Foundation in the form of a research fellowship. P. J. M. is also grateful to Daniel Holz for useful early discussions on double lenses and their likely frequency. Based on observations made with the NASA/ESA *Hubble Space Telescope*, obtained at the Space Telescope Science Institute, which is operated by the Association of Universities for Research in Astronomy, Inc., under NASA contract NAS 5-26555. This project would not have been feasible without the extensive and accurate database provided by the Sloan Digital Sky Survey (SDSS). Funding for the creation and distribution of the SDSS Archive has been provided by the Alfred P. Sloan Foundation, the Participating Institutions, the National Aeronautics and Space Administration, the National Science Foundation, the US Department of Energy, the Japanese Monbukagakusho, and the Max Planck Society. The SDSS Web site is http://www.sdss.org. The SDSS is managed by the Astrophysical Research Consortium (ARC) for the Participating Institutions. The Participating Institutions are the University of Chicago, Fermilab, the Institute for Advanced Study, the Japan Participation Group, Johns Hopkins University, the Korean Scientist Group, Los Alamos National Laboratory, the Max-Planck-Institute for Astronomy (MPIA), the Max-Planck-Institute for Astrophysics (MPA), New Mexico State University, University of Pittsburgh, University of Portsmouth, Princeton University, the United States Naval Observatory, and the University of Washington.

APPENDIX

DERIVATION OF THE PROBABILITY OF MULTIPLE LENSING

In this appendix we estimate the probability of finding a double lens in a sample of lenses like SLACS. The first ingredient is the surface density on the sky of potential lens galaxies, given by

$$N_{\rm gal} = \int d\sigma \int dz_l \frac{dn_l}{d\sigma} p(z_l) \frac{dV}{dz_l}, \tag{A1}$$

with dV/dz_l the comoving volume per unit solid angle and redshift and $dn_l/d\sigma$ the velocity dispersion function. For simplicity, we assume here that the shape of the velocity dispersion function does not evolve with redshift, but only in normalization as described by the $p(z_l)$ function. In practice, we consider the velocity dispersion function $dn/d\sigma$ measured by Sheth et al. (2003) at $z \sim 0.1$, which is of the form

$$\frac{dn_l}{d\sigma} = \phi_* \left(\frac{\sigma}{\sigma_*}\right)^{\alpha} \frac{\beta}{\sigma\Gamma(\alpha/\beta)} \exp\left[-\left(\frac{\sigma}{\sigma_*}\right)^{\beta}\right], \tag{A2}$$

with $\phi_* = 0.0020 \pm 0.0001\ h_{70}^3$ Mpc^{-3}, $\sigma_* = 88.8 \pm 17.7$ km s^{-1}, $\alpha = 6.5 \pm 1.0$, and $\beta = 1.93 \pm 0.22$.

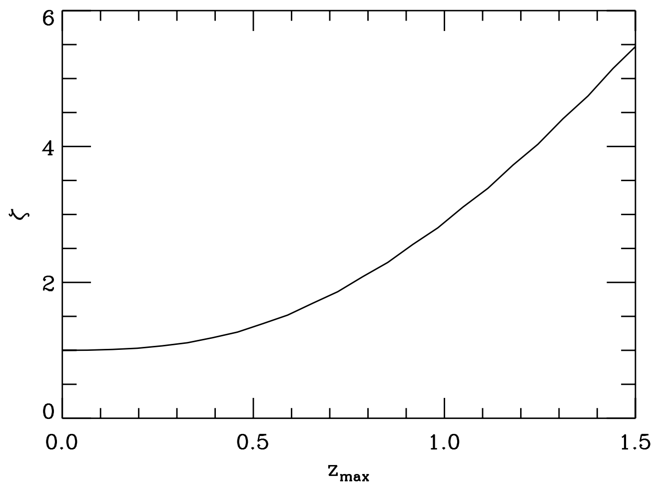

Fig. 12.—Evolution of the ζ term for multiple lensing probability boost $P(\text{lens } s2|\text{lens } s1)/P(\text{lens } s2)$ as a function of the limiting redshift $z_{\max}$ to which deflectors are considered.

The number density of foreground galaxies producing a single strong-lensing event on a source population $s1$ can be written as

$$N_{s1} = \int dz_{s1} \int d\sigma \int dz_l \frac{dV}{dz_l} \frac{dn_l}{d\sigma} p(z_l) \frac{dN_{s1}}{dz_{s1}} X(\sigma, z_l, z_{s1}), \tag{A3}$$

following Marshall et al. (2005). In this equation, $X(\sigma, z_l, z_{s1})$ is the cross section for lensing. In most cases of scale-free gravitational lenses $X(\sigma, z_l, z_{s1})$ can be separated such that $X(\sigma, z_l, z_{s1}) = \sigma^{2\nu} g(z_l, z_{s1})$, σ^ν giving the overall strength of the lens. For the particular case of a singular isothermal sphere that we consider, $\nu = 2$ and $g \propto (D_{\rm ls1}/D_{\rm os1})^2 \Theta(z_{s1} - z_l)$, with $\Theta(x)$ the Heaviside step function.

If the lensing cross section for a second population of sources $s2$ does not depend on the presence or properties of an already lensed population $s1$ galaxy, we can write

$$N_{s1,s2} = \int dz_{s2} \int dz_{s1} \int d\sigma \int dz_l \frac{dV}{dz} \frac{dn_l}{d\sigma} p(z_l) \frac{dN_{s1}}{dz_{s1}} \frac{dN_{s2}}{dz_{s2}} X_1(\sigma, z_l, z_{s1}) X_2(\sigma, z_l, z_{s2}). \tag{A4}$$

Combining equations (A1), (A3), and (A4) and taking advantage of the separability of the dependency on σ and on redshifts, the ratio of the probability that a galaxy lenses a source at z_{s2} given that it is already lensing a source at z_{s1} over the probability for a galaxy to lens a source at z_{s2} is given by

$$\frac{P(\text{lens } s2|\text{lens } s1)}{P(\text{lens } s2)} = \frac{P(\text{lens } s2,\ \text{lens } s1)}{P(\text{lens } s2)P(\text{lens } s1)} = \frac{N_{s1,s2} N_{\rm gal}}{N_{s2} N_{s2}} \tag{A5}$$

$$= \frac{\left[\int d\sigma (dn_l/d\sigma)\right]\left[\int d\sigma (dn_l/d\sigma)\sigma^8\right]}{\left[\int d\sigma (dn_l/d\sigma)\sigma^4\right]^2} \times \frac{\left[\int dV(z_l)p(z_l)\right]\left[\int dz_{s1}(dN_{s1}/dz_{s1}) \int dz_{s2}(dN_{s2}/dz_{s2}) \int dV(z_l)p(z_l)g(z_l, z_{s1})g(z_l, z_{s2})\right]}{\left[\int dz_{s1}(dN_{s1}/dz_{s1}) \int dV(z_l)p(z_l)g(z_l, z_{s1})\right]\left[\int dz_{s2}(dN_{s2}/dz_{s2}) \int dV(z_l)p(z_l)g(z_l, z_{s2})\right]} \tag{A6}$$

$$\equiv \Sigma \times \zeta, \tag{A7}$$

where $dV(z_l)$ indicates $(dV/dz_l)dz_l$. The first term Σ in equation (A6) describes the strong dependency of the lensing cross section on velocity dispersion. As expected because lensing favors high-σ systems, using the velocity dispersion function from Sheth et al. (2003), we estimate it to be larger than unity, of order $\Sigma = \Gamma[(8+\alpha)/\beta]\Gamma(\alpha/\beta)/\Gamma[(4+\alpha)/\beta]^2 \simeq 2.44$.

The second term ζ contains volume and lensing efficiency $g(z_l, z_s)$ effects that depend on the redshifts of the lens and the sources. By defining a lensing efficiency averaged over a given population of sources,

$$G_i(z_l) = \int dz_{si} \frac{dN_i}{dz_{si}} g(z_l, z_{si}), \tag{A8}$$

we can simplify the second term in equation (A6) and write it as

$$\zeta = \frac{\left[\int dV(z_l)p(z_l)\right]\left[\int dV(z_l)p(z_l)G_1(z_l)G_2(z_l)\right]}{\left[\int dV(z_l)p(z_l)G_1(z_l)\right]\left[dV(z_l)p(z_l)G_2(z_l)\right]}. \tag{A9}$$

To obtain a quantitative estimate of the probability of double lensing, let us consider some specific examples. The most important quantity in the definition of ζ is the comoving redshift distribution of deflectors $p(z_l)$. If all of them were confined in a single lens plane such that $p(z_l) = \delta(z_l - z_{l0})$, then $\zeta = 1$ and most of the change in probability comes from selection effects captured by Σ. If, instead, deflectors are broadly distributed over a range of redshifts, the ratio can be significantly higher than 1 because the probability of single lensing would be low for high-redshift deflectors, whereas the fact that a deflector is already lensing a source at z_{s1} favors lenses in a low-redshift range, more suitable for lensing a source at z_{s2}.

We illustrate this volume effect by assuming that the comoving density of deflectors is constant out to a redshift $z_{\max}$ and then drops to zero, that is, $p(z_l) = \Theta(z_{\max} - z_l)$. We also assume that the redshift distribution of background sources is of the form $dN/dz \propto e^{-z/z_0}(z/z_0)^{a-1}$. Population $s2$ galaxies follow the redshift distribution of faint background sources presented in Gavazzi et al. (2007) and having $z_0 = 0.345$ and $a = 3.89$. We use a redshift distribution for the $s1$ population that peaks around redshift 0.5, in agreement with the properties of spectroscopically discovered SLACS lenses (see Bolton et al. 2008). This corresponds to $z_0 \simeq 0.07$ and $a \simeq 7$. Note that the detailed shape of the redshift distribution for either $s1$ or $s2$ galaxies does not change the trends significantly, so this approximation is sufficient for our purposes. Figure 12 shows the evolution of ζ as a function of the limiting redshift $z_{\max}$. We see that, out to reasonable values $z_{\max} \simeq 0.5$, ζ does not depart much from unity.

To obtain a numerical value to be compared with our SLACS sample, we consider a population of deflectors constant out to redshift unity. The gain in probability is $P(\text{lens } s2|\text{lens } s1)/P(\text{lens } s2) \simeq 2.4$–5. In other words, if 1 elliptical galaxy at $z \lesssim 0.8$ in about 200 is strongly lensing a faint background source, a strong lens in approximately 40–80 is a double lens. This is consistent with the observations.

REFERENCES

Aldering, G., et al. 2004, preprint (astro-ph/0405232)
Barnabè, M., & Koopmans, L. V. E. 2007, ApJ, 666, 726
Bartelmann, M. 2003, preprint (astro-ph/0304162)
Bell, E. F., et al. 2006, ApJ, 640, 241
Blandford, R., & Narayan, R. 1986, ApJ, 310, 568
Bolton, A. S., Burles, S., Koopmans, L. V. E., Treu, T., & Moustakas, L. A. 2005, ApJ, 624, L21
———. 2006a, ApJ, 638, 703
Bolton, A. S., Burles, S., Schlegel, D. J., Eisenstein, D. J., & Brinkmann, J. 2004, AJ, 127, 1860
Bolton, A. S., Burles, S., Treu, T., Koopmans, L. V. E., & Moustakas, L. A. 2007, ApJ, 665, L105
Bolton, A. S., et al. 2006b, ApJ, 646, L45
———. 2008, ApJ, submitted
Brainerd, T. G., Blandford, R. D., & Smail, I. 1996, ApJ, 466, 623
Brewer, B. J., & Lewis, G. F. 2006, ApJ, 637, 608
Cabanac, R. A., et al. 2007, A&A, 461, 813
Casertano, S., et al. 2000, AJ, 120, 2747
Conroy, C., et al. 2007, ApJ, 654, 153
Dalal, N., Hennawi, J. F., & Bode, P. 2005, ApJ, 622, 99
Dye, S., Smail, I., Swinbank, A. M., Ebeling, H., & Edge, A. C. 2007, MNRAS, 379, 308
Dye, S., & Warren, S. 2007, preprint (astro-ph/0708.0787)
Gavazzi, R., Fort, B., Mellier, Y., Pelló, R., & Dantel-Fort, M. 2003, A&A, 403, 11
Gavazzi, R., et al. 2007, ApJ, 667, 176
Gerhard, O., Kronawitter, A., Saglia, R. P., & Bender, R. 2001, AJ, 121, 1936
Golse, G., Kneib, J.-P., & Soucail, G. 2002, A&A, 387, 788
Hoekstra, H., Hsieh, B. C., Yee, H. K. C., Lin, H., & Gladders, M. D. 2005, ApJ, 635, 73
Hoekstra, H., Yee, H. K. C., & Gladders, M. D. 2004, ApJ, 606, 67
Kochanek, C. S., & Narayan, R. 1992, ApJ, 401, 461
Kochanek, C. S., et al. 1999, in AIP Conf. Proc. 470, After the Dark Ages: When Galaxies Were Young (the Universe at $2 < z < 5$), ed. S. Holt & E. Smith (New York: AIP), 163
Koopmans, L. V. E. 2005, MNRAS, 363, 1136
———. 2006, in Engineering and Science, Vol. 20, ed. G. A. Mamon et al. (Les Ulis Cedex: EDP Sciences), 161
Koopmans, L. V. E., Treu, T., Bolton, A. S., Burles, S., & Moustakas, L. A. 2006, ApJ, 649, 599
Leauthaud, A., et al. 2007, ApJS, 172, 219
Mandelbaum, R., Seljak, U., Kauffmann, G., Hirata, C. M., & Brinkmann, J. 2006, MNRAS, 368, 715
Marshall, P., Blandford, R., & Sako, M. 2005, NewA Rev., 49, 387
Marshall, P. J., et al. 2007, ApJ, 671, 1196
Moran, S. M., et al. 2007, ApJ, 665, 1067
Moustakas, L. A., et al. 2007, ApJ, 660, L31
Myers, S. T., et al. 2003, MNRAS, 341, 1
Oyaizu, H., et al. 2008, ApJ, 674, 768
Peng, C. Y., Ho, L. C., Impey, C. D., & Rix, H. 2002, AJ, 124, 266
Prada, F., et al. 2003, ApJ, 598, 260
Ratnatunga, K. U., Griffiths, R. E., & Ostrander, E. J. 1999, AJ, 117, 2010
Réfrégier, A., et al. 2006, Proc. SPIE, 6265, 58
Rubin, V. C., Peterson, C. J., & Ford, W. K., Jr. 1980, ApJ, 239, 50
Schlegel, D. J., Finkbeiner, D. P., & Davis, M. 1998, ApJ, 500, 525
Schneider, P., Ehlers, J., & Falco, E. E. 1992, Gravitational Lenses (Berlin: Springer)
Sheldon, E. S., et al. 2004, AJ, 127, 2544
Sheth, R. K., et al. 2003, ApJ, 594, 225
Soucail, G., Kneib, J.-P., & Golse, G. 2004, A&A, 417, L33
Suyu, S. H., Marshall, P. J., Hobson, M. P., & Blandford, R. D. 2006, MNRAS, 371, 983
Swaters, R. A., Madore, B. F., van den Bosch, F. C., & Balcells, M. 2003, ApJ, 583, 732
Treu, T., & Koopmans, L. V. E. 2002, ApJ, 575, 87
———. 2004, ApJ, 611, 739
Treu, T., Koopmans, L. V., Bolton, A. S., Burles, S., & Moustakas, L. A. 2006, ApJ, 640, 662
Trujillo, I., Burkert, A., & Bell, E. F. 2004, ApJ, 600, L39
van Albada, T. S., Bahcall, J. N., Begeman, K., & Sancisi, R. 1985, ApJ, 295, 305
Warren, S. J., & Dye, S. 2003, ApJ, 590, 673
Warren, S. J., et al. 1996, MNRAS, 278, 139
Wayth, R. B., & Webster, R. L. 2006, MNRAS, 372, 1187